How well do discrete element granular flow models capture the essentials of mixing processes?

Paul W. Cleary[1], Guy Metcalfe[2] and Kurt Liffman[2]

[1] CSIRO Division of Mathematical and Information Sciences, Clayton, Victoria.
[2] CSIRO Division of Building, Construction and Engineering, Highett, Victoria.

ABSTRACT

Flowing granular materials, undergoing both mixing and segregation, play important roles in industries ranging from minerals and food to pharmaceuticals and ceramics. Sometimes it is desirable to enhance the mixing and inhibit segregation and in other cases it is desirable to minimise the mixing and enhance the segregation. The fundamentals of these processes are poorly understood. Computational modelling of such granular flows offers an good opportunity to study these fundamentals. But how well do these discrete element based modelling techniques capture the essential features of mixing processes?

The capabilities of our discrete element modelling package are described. Two different methods for measuring the rates of mixing are presented and three different configurations are studied. Qualitatively reasonable flows are obtained. A detailed study of the mixing demonstrates that the amount and nature of the mixing is quite sensitive to a range of physical parameters.

1. NOMENCLATURE

A - mean value of distribution a_i
h - fill level of the tumbler: range [0,1]
m_i - weighting of ith value in distribution
$M = \sum_i m_i$ N - number of particles
n_a - ave number of particles in a local average
R - tumbler radius = 15 cm
ϵ - Coefficient of restitution
η - coefficient of variation ω - rotation rate
μ - Surface friction σ - standard deviation

2. OVERVIEW OF PACKAGE

CSIRO's Division of Mathematical and Information Sciences has developed a two dimensional package based on a discrete element method. It consists of a graphical pre-processor that is used to construct the problem geometry, a main simulation code and a range of post-processing programs that are used to analyse the flows.

Boundary objects of nearly arbitrary shape are constructed from line, circular or disc primitives. Flows in the complex geometries found in industrial applications can then be modelled. Rigid body and surface motions can be specified and external forces can be attached. The particles are modelled as discs. Packed particle microstructures are built by filling user specified polygons with particles having any size and density distributions.

The main code uses the pre-processor and other information to perform the required simulation. The flows can then be analysed with an array of visualisation and data processing tools to provide information such as wear rates and distributions, collision forces, dynamic loads on boundaries, sampling and flow statistics, mixing and segregation rates.

3. THE SIMULATION METHOD

The modelling technique is a soft particle method. The particles are allowed to overlap and the amount of overlap Δx, and the normal and tangential relative velocities determine the collisional forces. Figure 1 illustrates the collisional forces. The normal force F_n has a spring to provide the repulsive force that pushes the particles apart and a dashpot that provides dissipation, resulting in an effective coefficient of restitution. The tangential component has an incrementing spring and dashpot that is subject to the frictional limit.

The algorithm can be briefly summarised as having three key parts:

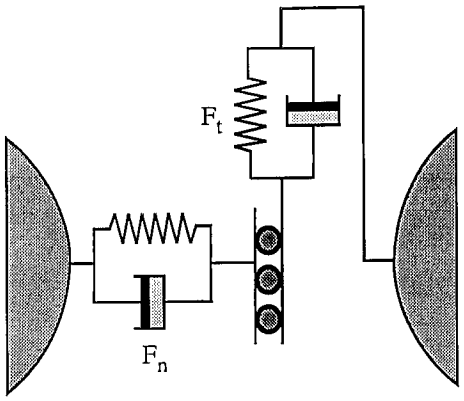

Δx is the particle overlap,
k is the spring constant
v_n and v_t are the normal and tangential velocities,
C is the dashpot damping coefficient
μ is the friction coefficient

Normal Force $\quad F_n = -k\Delta x + Cv_n$

Tangential Force $\quad F_t = \min(\mu F_n, \int k v_t dt + Cv_t)$

Figure 1: The contact force model involves a spring and a dashpot in parallel in the normal direction and a spring limited by the sliding friction in the tangential direction.

- A search grid is used to build a near-neighbour interaction list. The boundary objects appear as virtual particles.
- The collisional forces on the particles and boundaries are evaluated efficiently using the near-neighbour list and the spring-dashpot interaction model.
- All the forces on the objects and particles are summed and the resulting equations of motion are integrated.

It has been successfully used to model a wide range of industrial and geophysical applications (see Cleary 1994, 1996 and Campbell 1990 for references).

4. MEASURING MIXING

We have developed a method to measure mixing and segregation in granular flows with continuous or complex particle distributions. It does not rely on any spatial correlations, is very flexible and can be used for many industrial applications. It is based upon taking local averages of the desired property, (such as mass, density, diameter or colour). The probability distribution of these local averages characterises the extent of mixing. This distribution can be described uniquely by its coefficient of variation η which is given by the ratio of the standard deviation to the mean. This mixing measure is not unique. Poux *et. al.* (1991) contains a range of other such measures.

The essential elements of the algorithm are:

- A suitable averaging box is chosen (dimensions in multiples of r_{min}). For flows where the mixing or segregation is two dimensional (in cylindrical tumblers) the averaging box should be square. For one dimensional mixing/segregation (in a vibrating box), a wide but short box gives fine resolution in the vertical direction and complete averaging in the other. A suitable box can be chosen for each application. The box needs to be large enough so that the average is meaningful, but small enough so that useful amounts of information about spatial variations remain.
- An $n_x \times n_y$ grid is placed over the part of the flow domain of interest.
- A local average is calculated using all the particles contained within the averaging box centered on each grid point.
- Local averages with insufficient points to be meaningful are discarded.
- The probability distribution for the local averages is constructed.
- The mean, standard deviation and η of the distribution are calculated. These vary with time allowing us to estimate mixing and segregation rates.
- Estimates of the coefficients of variation for the randomly mixed case η_r and fully segregated case η_s are made. The variance of a randomly mixed granular material is:

$$\sigma^2 = \left(\frac{N}{n_a} - 1\right) \sum_i \left(\frac{m_i}{M}\right)^2 (a_i - A)^2 .$$

- The fully segregated case is given by the probability distribution of the selected property across the individual particles.
- The state of mixing or segregation is then characterised by $\xi = (\eta - \eta_r)/(\eta_s - \eta_r)$.

Figure 2 shows the case of a randomly mixed set of particles. a) shows the particles and b) the distributions. The particle radius is approximately uniformly distributed from 0.75 to 1.5 mm. This is shown by the some-

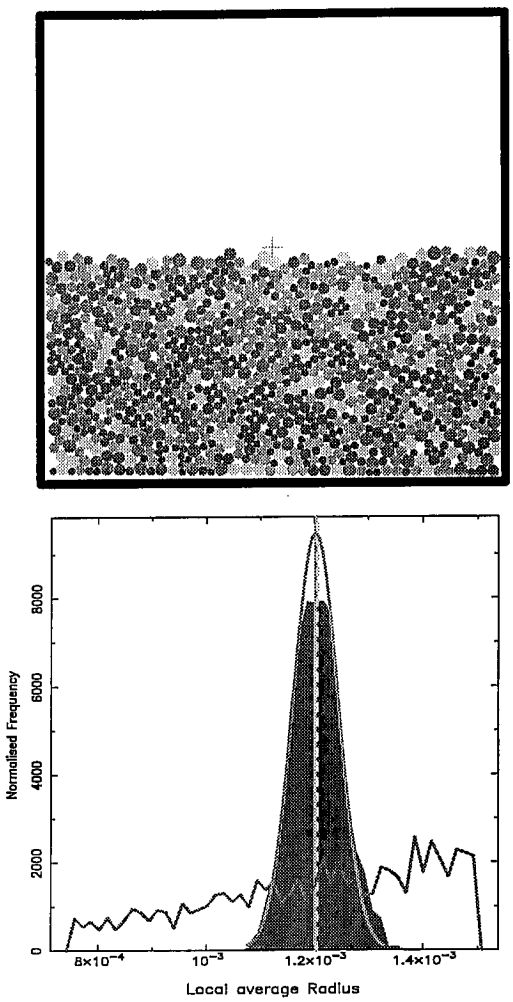

Figure 2: a) Random mixture of particles b) Distribution of local average particle radius.

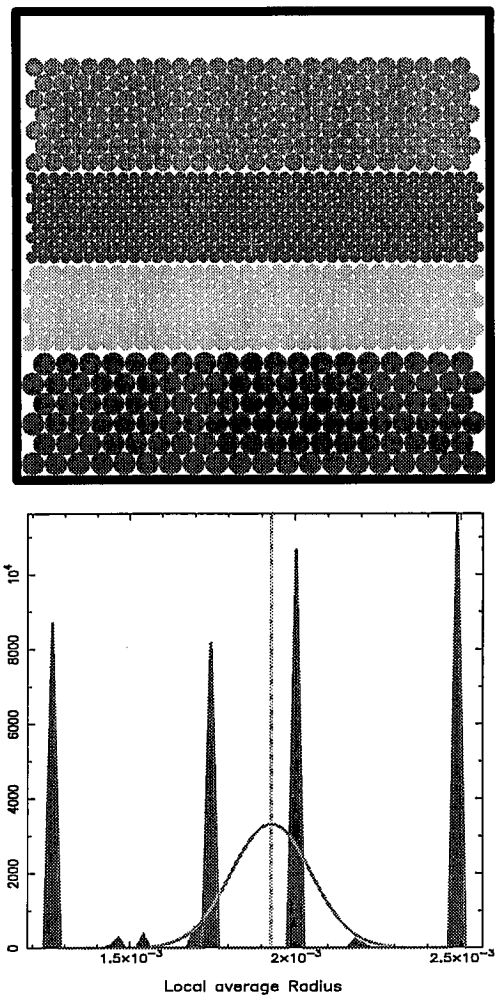

Figure 3: a) Four fully segregated layers b) Distribution of local average particle radius.

what jagged and almost horizontal line. The vertical light grey line at 1.25 mm is the mean particle size. The light grey bell shaped curve is the predicted distribution of local average radius for the randomly mixed case. The dark shaded area is the actual local average distribution calculated. Note that this distribution is very close to that of the randomly mixed case. Its peak is a little shorter and its right edge extends slightly beyond that of the randomly mixed curve. This shows that the local average approach can identify mixtures that are very close to the theoretically randomly mixed case. Here the difference is only 3%.

Figure 3 shows fully segregated particles lying in four distinct layers. a) shows the particle layers and b) shows the relevant distributions. The light grey dashed vertical line is the mean radius. The light grey bell curve is the randomly mixed limit. The fully segregated limit is the mid grey line with four separate peaks, one for each of the layers. The actual local average distribution is the dark grey shaded area. This is almost indistinguishable from the curve delimiting the fully segregated limit. Note that there are three very small peaks between the main ones. This is the full extent of the aliasing produced by the local averages for the boxes that contain two different sizes of particles. $\xi = 0.97$ is only 3% from the fully segregated limit.

This technique is able to identify both the fully segregated and randomly mixed limits with high accuracy. It produces little aliasing of real peaks if the averaging box is chosen properly. It is a sensitive tool for analysing subtle variations in the mixing states.

5. MIXING IN A ROTATING BOX

We use the above method to analyse the changing state the mixture shown in Figure 3a when the box spins about its center at 15

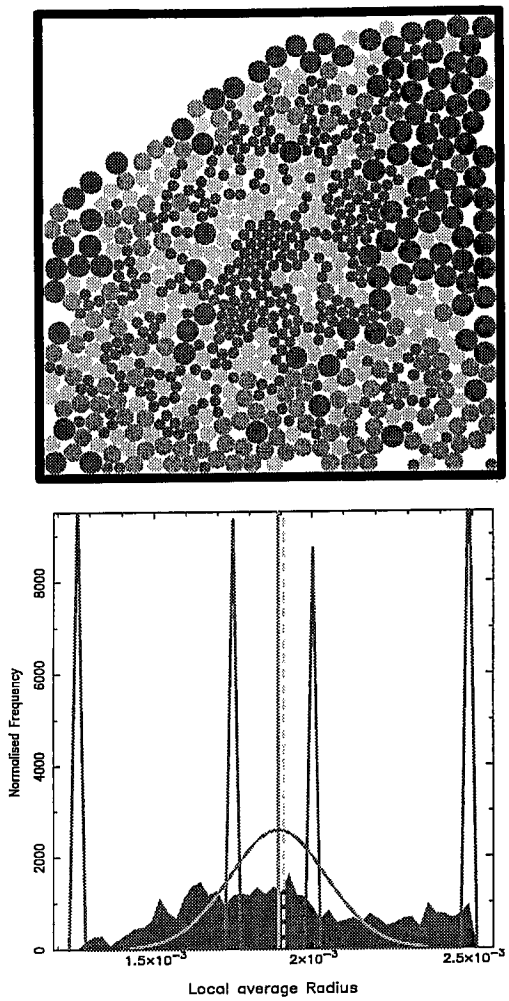

Figure 4: At $t = 35$. a) Particle positions show a moderate mixing b) Distribution of local average particle radius is much flatter.

rpm. This motion causes the top surface to become inclined. The angle of the surface is maintained by a sequence of avalanches, which slowly mix the particles.

Figure 4a shows the particles after 8.75 revolutions. There has been a substantial amount of mixing but the mixing is not complete or global. A core of the smallest particles has formed and few of them are near the boundaries. The largest particles are predominantly on the right side and along the top. The second largest size (mid grey) are predominantly in the bottom half of the box, whilst the second smallest size are fairly well uniformly distributed. Figure 4b shows the distributions at $t = 35$. The randomly mixed and segregated limits are shown as usual. The four sharp initial peaks in the distribution (Figure 3b) have disappeared as the particles mix. Conversely the distribution is still quite some distance from the randomly mixed state. The uniform extension of the distribution beyond the right tail of the bell curve out to 2.5 mm is produced by the fairly unmixed large particles. Similarly, the smaller peak near 1.25 mm is produced by the central core of small particles. In between, the distribution has formed a bell shape centered on 1.8 mm. This reflects the well mixed remainder of the particles.

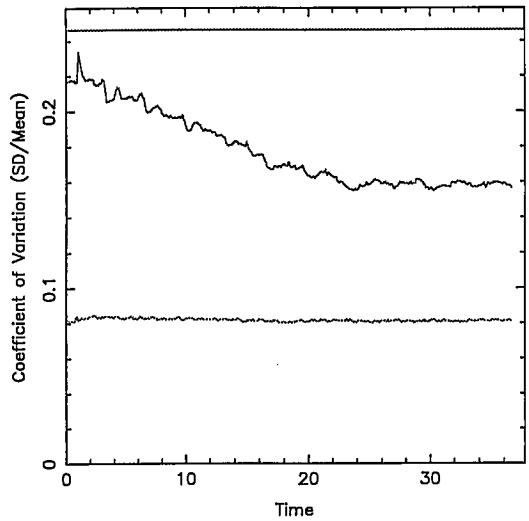

Figure 5: Time variation of η for the local averages (middle curve), fully segregated (upper) and randomly mixed (lower) cases.

Figure 5 shows the time variation of η. The central line corresponds to the state of the mixture, while the upper and lower curves are the normal limit cases. η starts from close to the fully segregated value and trends down linearly until $t = 24$. This indicates a constant rate of mixing. The fluctuations are produced by the avalanching of the surface particles. At $t = 24$ there is an abrupt change and there is no further mixing. It is unsound to assume that mixing will continue to the random limit. This example demonstrates that our mixing measurement methodology can easily and clearly detect the presence of mixing, can determine its rate and its cessation. Similarly, it can monitor segregation.

6. A 60% LOADED TUMBLER

Next we examine the flow pattern in a 30 cm diameter cylinder (tumbler) loaded to 60% of its volume and rotating at 2.4 rpm. The particles have approximately uniform size with mean diameter 2 mm. $\epsilon = 0.5$ and

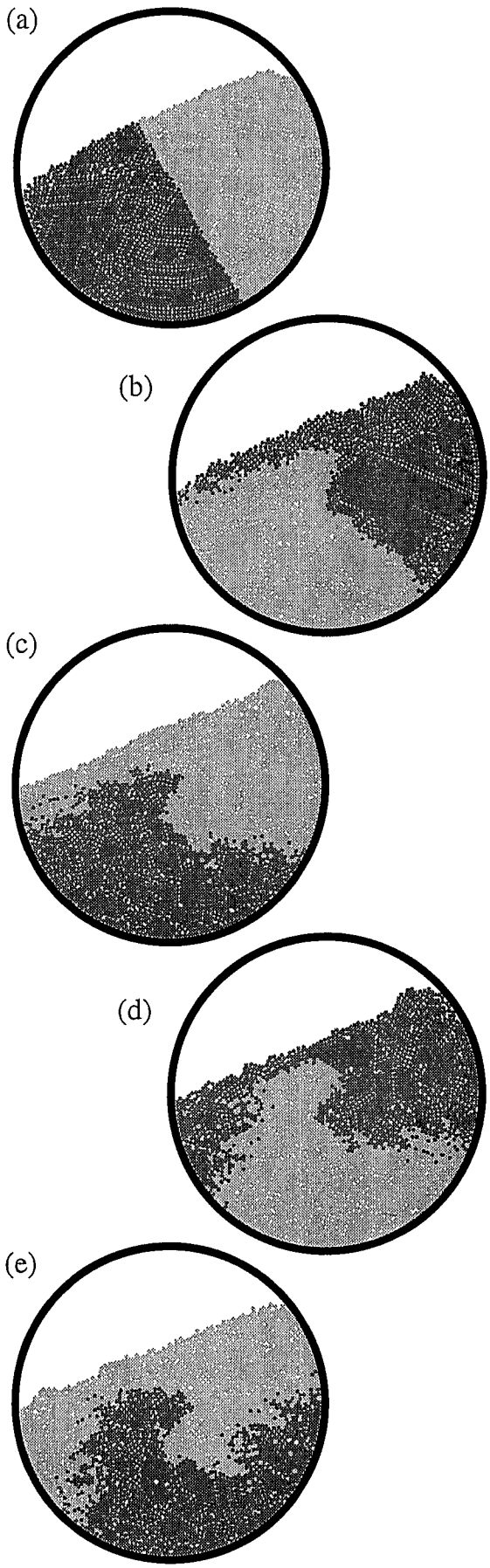

Figure 6: Mixing in a 60% loaded tumbler, a) $t = 2$ s, b) $t = 12$ s, c) $t = 22$ s, d) $t = 32$ s and e) $t = 42$ s

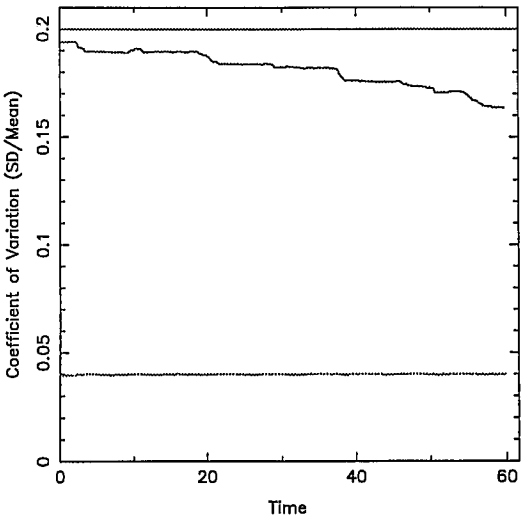

Figure 7: Mixing in a 60% loaded tumbler.

$\mu = 0.75$. This approximately matches the experimental setup of Metcalfe *et. al.* (1995).

Figure 6 shows snapshots of the flow. The particles are shaded (coloured) differently on the two sides of the tumbler in order to track the mixing. Frame a) shows the particles rotating as a rigid mass. This is demonstrated by the undeformed surface of the material and the line separating the two colours. At around $t = 3$ the angle of the surface exceeds the angle of failure and the material above this begins to avalanche. The particle motion is relatively simple: they rotate as a rigid mass until above the angle of failure and flow down the slope as a series of discrete avalanches. The demarcation between the two sets of particles is unchanged by any avalanches that consist of only one colour. If the boundary between the two regions passes through the thin avalanching layer or intersects the top surface then particles of both colours are able to mix.

The depth of the cascading layer is around 6 to 7 particles. This is consistent with the experiments. For fill levels higher than $h = 0.5$ or a 50% loading the particles near the center never participate in the surface avalanching. This is observed experimentally to lead to a precessing core of unmixed material. This can be also be clearly seen developing in the simulations. Figure 6b shows the configuration after light grey (red) material has flowed once over the surface of the dark grey (blue) material which is in turn just flowing back down over the light grey (red) material. The interface between the two materials has become

bent. The central (almost vertical section) delimits the non-mixing core. Subsequent frames show the state after light grey material has again flowed over the dark and then alternatingly back and forwards. With each exchange the interfaces become more curved and more diffuse. The mixing is very slow for these loadings. The non-mixing core becomes better defined in each frame.

Figure 7 shows our mixing measure. The upper and lower lines are the usual limit cases. The middle line shows the present state of the system. It indicates that the material is initially close to fully segregated. The mixing then occurs as a series of downward steps. Each corresponds to an avalanche in which both colours are mixed. The cumulative effect of these small mixing avalanches leads to very slow, progressively better mixing. By $t = 60$ (2.4 revolutions) the materials are about 25% of the way to being fully mixed. As the materials become better mixed the step-like nature of the mixing becomes progressively more continuous.

Overall, this simulation shows many qualitative similarities to the experiments. The mixing at this fill level is very slow and we detect a precessing non-mixing core. The avalanches are also about the correct depth.

7. CENTROID MEASURE

An alternative mixing measure for such tumbler experiments uses changes in the location of centroids of the two different materials. This was developed by Metcalfe *et. al.* (1995) for experiments and simulations.

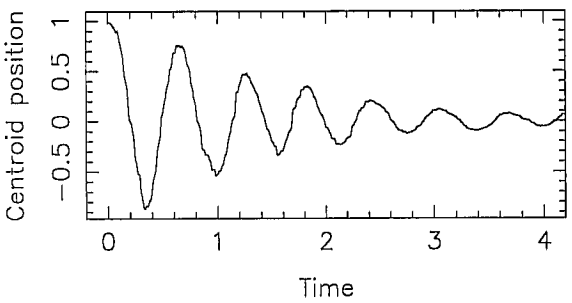

Figure 8: Time variation of centroid location for light grey particles on right of the tumbler.

The motion of the centroids of the two types of particles set up in this way is sinusoidal with an exponentially decaying envelope. Figure 8 shows an example. The centroid location has the location of the centroid of all the particles subtracted and is scaled by its initial value. The time is shown in revolutions of the tumbler. The circulatory motion of the particles causes the two materials to exchange sides on the tumbler with a characteristic period T. The decay of the envelope is caused by the mixing. This time series for the x coordinate of the centroid position can be well approximated by:

$$x_c = e^{-\gamma t} \cos\left(\frac{2\pi t}{T}\right)$$

The values of T and γ then characterise the mixing. For this case $\gamma = 0.7$ and $T = 0.61$.

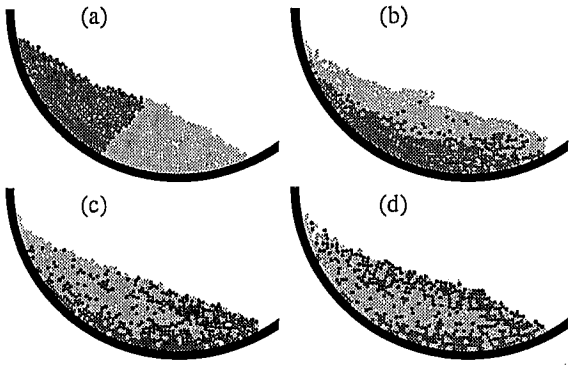

Figure 9: Mixing for $h = 0.2$ at a) 0.01, b) 0.5, c) 1.0 and d) 1.5 revolutions.

Figure 9 shows snapshots of the mixing that produced the centroid trace in Figure 8. Note the rapid mixing of particles of one type into the mass of the other particles.

8. COMPARISON VALIDITY

Comparison of these simulations and the experiments is difficult for two reasons:

- The material properties of the material and the liner are not well known and the results depend sensitively on them. An understanding of the sensitivity of the simulation results is essential to understanding the multi-dimensional parameter space in which these experiments lie.
- The simulation configurations are highly idealised. It is not a priori clear if all these idealisations are valid. Some may not affect the overall dynamics whereas other may affect them significantly. This raises the question as to which approximations are reasonable and how to model the details that are important?

A study of the sensitivity of γ and T to various physical parameters follows.

9. MIXING RATES

A series of simulations was performed to identify the effects of various physical parameters on the mixing. The base conditions were $\omega = 6$ rpm, $\mu = 1.0$, $\epsilon = 0.5$, particle mean size of 1.8 mm and a size variation of $\pm 2.4\%$.

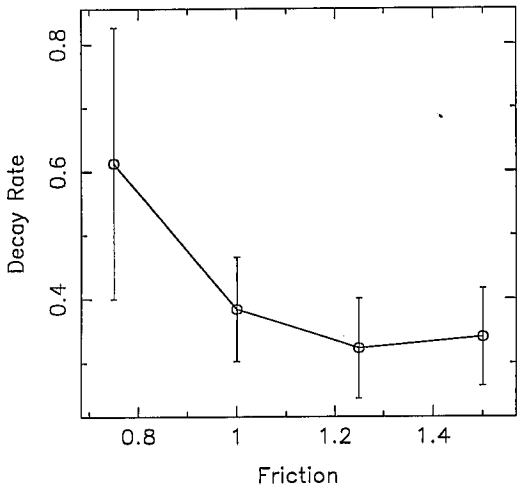

Figure 10: Variation of γ with μ.

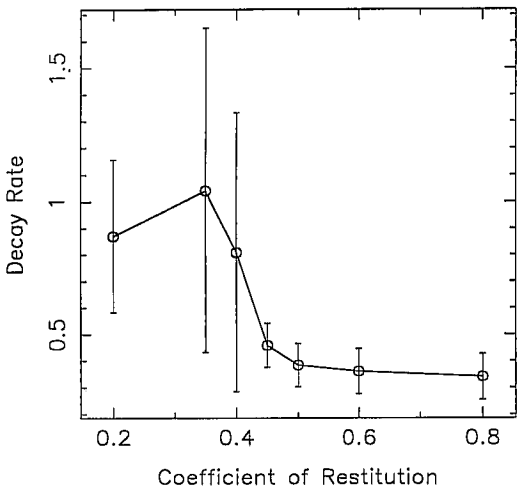

Figure 11: Variation of γ with ϵ.

Figures 10-12 show the behaviour of γ with changes in μ, ϵ and the size distribution. Both γ and T are relatively constant for $\mu \geq 1$ and both increase for lower values. This is caused by the flow developing a partially slumping and partially circulating motion. This speeds the mixing but slows the centroid exchange. There is a surprising sensitivity to ϵ. For $\epsilon \geq 0.5$, both γ and T are relatively constant. For lower values (increasingly dissipative flows) both γ and T increase sharply. There is also an abrupt increase in the error ranges. For very low ϵ the flows develop a hump towards the bottom of the down slope as the avalanches have insufficient energy to reach the bottom of the tumbler in one movement. This seems to be connected to the increase in T. The mixing is relatively insensitive to small size variations in the particle sizes (Figures 12). Once the size variation reaches $\pm 20\%$ of the mean size, it begins to strongly affect the mixing rate which nearly doubles. The mixing period T steadily declines as the size variation increases.

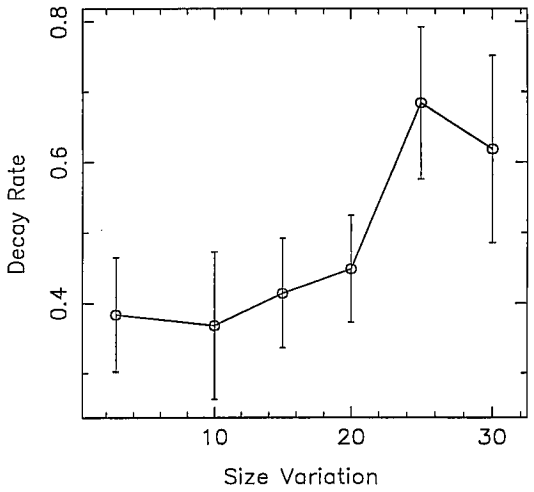

Figure 12: Variation with particle size range.

Further tests indicate that values of rolling friction as high as $0.025\,g$ have no effect. This indicates that the frictional connection between the particles and the tumbler are already sufficient to prevent any sliding along the tumbler wall. A lower dynamic friction coefficient than the static one slightly increases both γ and T. Conversely, the rotation rate has a significant effect on the mixing rate by changing the flow regime. A slower rotation rate of 2.4 rpm gives γ about 35-65% larger than those for 6 rpm.

To check the numerical accuracy, four times the spring stiffness was used. This reduces the particle overlaps by a factor of four and is roughly the equivalent of mesh refinement for discrete element methods. There was no change in mixing rate or period.

10. EXPERIMENT COMPARISON

The experimental results for $h = 0.2$ gave $\gamma \approx 2.5$ and $T \approx 0.23$. These were obtained for cubic salt particles with a mean size of 1.01 mm, a size range of $\pm 20\%$ and a tumbler rotation of 2.5 rpm. The values of μ and ϵ are unknown. Our simulation overturning period

T is about 2-3 times this and the mixing rate is about eight times our base case and about three times our closest result (for low values of ϵ and ω). Combinations of lower ϵ and $\omega = 2.4$ rpm will give still closer results.

Qualitatively, our simulated flow patterns, for both $h = 0.2$ and a 60% load, are very similar to those of the experiments. Quantitatively, there is a sizable gap for the $h = 0.2$ case. The essential difference seems to lie in the size of the overturning period. If all the particles away from the surface avalanching layer are moving rigidly with the tumbler then the period should theoretically be around 0.25. Our longer period indicates that our particles are not in such a state. Rather our flow consists of a slow slumping deformation as well as the circulatory flow. This indicates that the material strength is too low. Surprisingly, increases in the friction cannot explain this discrepancy. Increasing the size variation increases the microstructure strength and was observed to decrease the overturning period and increase the mixing rate. The most likely reason for the disrepancy is our use of circular particles to approximate salt cubes. This suggests that neglecting particle shape may have a significant effect on the mixing behaviour. Additionally, the use of circular particles limits the angle of repose to 22^o. This shallower angle reduces the kinetic energy in each avalanche leading to a significantly lower mixing rate. Finally, three dimensional microstructures are stronger than two dimensional ones. Part of the reduced material strength may relate to the two dimensionality of the simulations.

11. CONCLUSIONS

Mixing of granular materials in rotating tumblers was studied using a discrete element modelling method. Two methods were presented for measuring mixing and segregation rates. The first involves the calculation of local averages and characterising the resulting distribution by its coefficient of variation. This method is valid for all particle distributions. The second involves following the relative location of the centroid of a class of particles. This is suited for particles belonging to discrete classes. The centroid motion is a decaying oscillation. The decay rate and the oscillation period completely characterise the mixing.

Qualitatively, the simulation flow patterns are similar to the experiments. The slow mixing rates and the existence of a precessing non-mixing core were found for $h > 0.5$. Faster mixing and the circulatory flow were also obtained for lower fill levels. Quantitatively, there is a significant difference between the actual mixing rates for $h = 0.2$. The most likely cause is in neglecting the real shape of the particles. The cubic shaped salt crystals are expected to have much stronger microstructures than circular particles. This shows that the collective strength of particle clusters can be much more important than the individual particle interactions. It is also clear that lack of information about material properties is a handicap to validation.

A parametric study indicates that mixing increases strongly for $\epsilon < 0.5$ and $\mu < 1.0$. It also increases with the size variation of the particles, particularly above $\pm 20\%$ as the microstructures become stronger. The mixing rate also increases strongly with lower rotation rates. Rolling friction is unimportant and having a lower dynamic friction coefficient increases the mixing rate only slightly.

REFERENCES

Campbell, C. S., 1990, "Rapid Granular Flows", *Annual Rev. Fluid Mech*, **22**, pp 57-92.

Cleary, P. W., "Design and Loading of Dragline Buckets", *Proc. MISG*, 1993, pp. 39-67.

Cleary, P. W., "Modelling granular flows with complex boundary geometries", 1993, *Proc. 6th Int. Comp. Tech. & Appl. Conf.*, Eds. Stewart, D., Gardener, H., and Singleton, D., pp 148-155.

Cleary, P. W., 1994, "Modelling industrial granular flows", *Proc. 1st Aust. Eng. Math. Conf.*, pp. 169-177, Melbourne, Eds. A. K. Easton and J. M. Steiner, Studentlitteratur.

Cleary, P. W., 1996, "Discrete element modelling industrial granular flows", to appear: *Proc. 2nd Aust. Eng. Maths. Conf.*, Sydney.

Metcalfe, G., Shinbrot, T., McCarthy, J. J., and Ottino, J. M., 1995, "Avalanche mixing of granular solids", Nature, **374** 39-41.

Poux, M., Fayolle, P., Betrand, J., Bridoux., D., and Bousquet, J., 1991, "Powder mixing: some practical rules applied to agitated systems", *Powder Technology*, **68**, 213-234.